

# 3D Printing and Additive Manufacturing

Q1

Industrial and Manufacturing Engineering

best quartile

SJR 2022

0.72



powered by scimagojr.com

## Quartiles





# *In Situ* Wire + Powder Synchronous Arc Additive Manufacturing of Ti–Cu Alloys

Chuanchu Su,<sup>1,2</sup> Yanhu Wang,<sup>1–3</sup> Weimin Wu,<sup>1</sup> Sergey Konovalov,<sup>1,2</sup> Lei Huang,<sup>1,2</sup> Xizhang Chen,<sup>1–3</sup> and Shuyang Qin<sup>4</sup>

## Abstract

In this study, a new wire + powder synchronous arc additive manufacturing technique was used to manufacture Ti–Cu alloys. The microstructure and properties of the as-fabricated alloys were studied. The results showed that the prepared Ti–Cu alloys have good properties. The Cu with high growth restriction factor can increase the constitutional supercooling zone in the Ti–Cu alloys, which can override the negative effect of a high thermal gradient in the manufacturing process. Through the observation of the microstructure, the as-printed Ti–Cu alloy specimens have equiaxed fine-grained microstructure. Through corrosion performance analysis, the Cu can also make the passivation film of the alloy more compact and make the alloy more corrosion resistant.

**Keywords:** additive manufacturing, wire+ powder, Ti–Cu alloys, mechanical properties, corrosion

## Introduction

ADDITIVE MANUFACTURING (AM) PROVIDES an effective method to fabricate complex structural components with multiple materials.<sup>1–4</sup> Wire–arc additive manufacturing (WAAM) is a cheaper AM method than electron beam melting and selective laser melting methods.<sup>5–7</sup> WAAM offers a high arc column temperature, high deposition efficiency, and high handling mobility, which is suitable for manufacturing large structures with multiple materials.<sup>8–10</sup> However, alloys produced by WAAM have low surface precision.<sup>11,12</sup> The surface precision of the samples produced by powder feeding arc AM is high with the appropriate process and parameters, but the utilization rate of powder is low, which easily causes dust pollution.<sup>13–15</sup>

In view of the mentioned analysis, we propose wire + powder synchronous arc AM. Combined wire + powder synchronous arc AM is based on an arc as the heat source, and wire and powder material are simultaneously filled in the molten pool. The deposition is performed layer by layer to achieve AM. It is a new AM technology. Wire + powder

synchronous arc AM combines the advantages of the two technologies.

It has the advantages of high efficiency, high density, and flexible adjustment and is suitable for the additive preparation of metal matrix composites and functionally graded materials.<sup>16–18</sup> The addition of wire is conducive to increasing the area of the deposited layer, providing a way to manufacture complex structural parts and improving the preparation efficiency and material density. The addition of powder can provide a reinforcing phase, and a metal composite material with a gradient composition of the particle reinforcing phase can be prepared.

More importantly, the wire + powder synchronous arc AM can inhibit the segregation that Ti–Cu alloys easily exist during the solidification process, so it is favorable for making Ti–Cu alloys. A new method for preparing titanium alloy has been developed.<sup>19</sup>

Ti–Cu alloys have excellent corrosion resistance, strong antibacterial properties, and high strength, which are widely used in the petroleum, chemical, metallurgy, biomedicine, and aerospace industries.<sup>20</sup> For Ti–Cu alloys, the addition of

<sup>1</sup>Zhejiang Provincial Key Laboratory of Laser Processing Robotics, College of Mechanical and Electrical Engineering, Wenzhou University, Wenzhou, China.

<sup>2</sup>Department of Mechanics and Engineering, Siberian State Industrial University, Novokuznetsk, Russia.

<sup>3</sup>China International Science & Technology Cooperation Base for Laser Processing Robotics, Wenzhou University, Wenzhou, China.

<sup>4</sup>National Engineering Research Center for Equipment and Technology of Cold Strip Rolling, Yanshan University, Qinhuangdao, China.

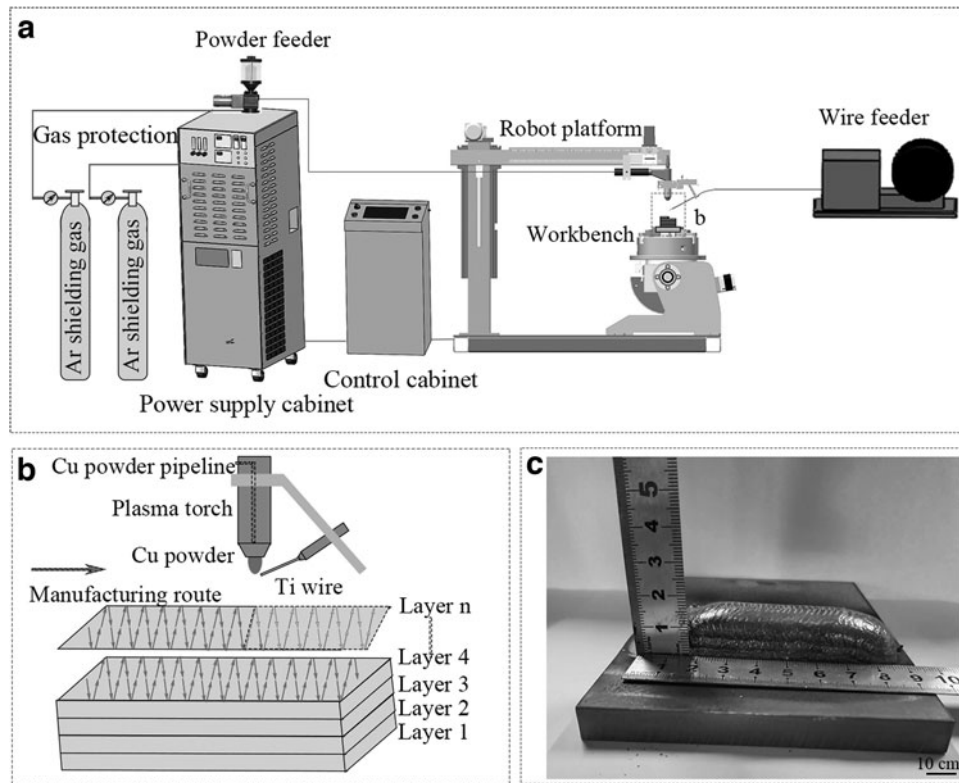


FIG. 1. Illustration of the wire + powder synchronous arc additive manufacturing setup (a), illustration of deposition (b), and as-deposited Ti-7.3%Cu sample (c).

Cu provides a wider  $\beta$ -phase transition zone on the Ti-rich side of the Ti-Cu phase diagram, which can form various forms of intermetallic compounds so that they have different features to meet the application of different occasions.<sup>20-25</sup> Although Ti-Cu alloys are a very promising material, the casting of Ti-Cu is particularly difficult due to its high melting temperature and high reactivity with oxygen, and it is prone to segregation and dendrites during casting.

Moniri Javadhesari et al. and Liu et al.<sup>26,27</sup> studied the relationship between copper content and antibacterial property of Ti-Cu alloys. The content of copper had a great impact on antibacterial properties, but did not study the effect on mechanical properties. Hayama et al., Holden et al., and Williams et al.<sup>20,28,29</sup> studied the effect of heat treatment on the mechanical behavior of Ti-Cu alloys. Their research showed that the cooling rate affects the phase transformation, which had a major impact on mechanical properties. These studies give us two inspirations. If we want to obtain high performance Ti-Cu alloys, we can start with copper content and technology.

Metal AM process has two main characteristics: high cooling rates and high thermal gradient, which often lead to two completely different phenomena: one is very fine microstructure, and the other is almost exclusively columnar grains.<sup>30</sup> Cu as a solute element has high growth restriction factor  $Q$ , and a supercooled zone can be formed. According to interdependence theory, if the composition of the supercooled zone is larger, the grain will be easier to refine.<sup>31</sup> Therefore, using this method to manufacture Ti-Cu alloys is more prone to fine equiaxed grains. It solves the segregation in the casting process and the inherent large columnar crystal defect in AM.

In this research, wire + powder synchronous arc AM was used to manufacture Ti-Cu alloys. We used pure Ti wire ( $\geq 99.9\%$ ) and pure Cu powder ( $\geq 99.99\%$ ) as raw materials. Ti wire is used to provide a dense titanium matrix, and Cu powder is used to refine the grain and increase the reinforcing phase. We studied the properties of Ti-7.3%Cu alloys prepared by wire + powder synergistically by controlling the wire feeding speed and feeding amount.

## Experiment

### Process and equipment introduction

The wire + powder synchronous arc AM setup is shown in Figure 1a. The AM process is shown in Figure 1b. It mainly includes powder plasma arc additive manufacturing (PPA-

TABLE 1. WIRE + POWDER SYNCHRONOUS ARC ADDITIVE MANUFACTURING PROCESS PARAMETERS

| Parameter                                | Value | Unit       |
|--|-------|------------|
| Deposition current                       | 105   | A          |
| Pulse period                             | 63    | $\mu$ s    |
| Cu powder feed velocity                  | 0.7   | g/min      |
| Ti wire speed                            | 8.9   | g/min      |
| Travel speed                             | 400   | mm/min     |
| Shielding Ar gas                         | 10    | L/min      |
| Powder feeding Ar gas                    | 3.5   | L/min      |
| Dwell time between deposition layers     | 2     | min        |
| Angle between the torch and filler wire  | 60    | $^{\circ}$ |
| Distance between the torch and workpiece | 15    | mm         |

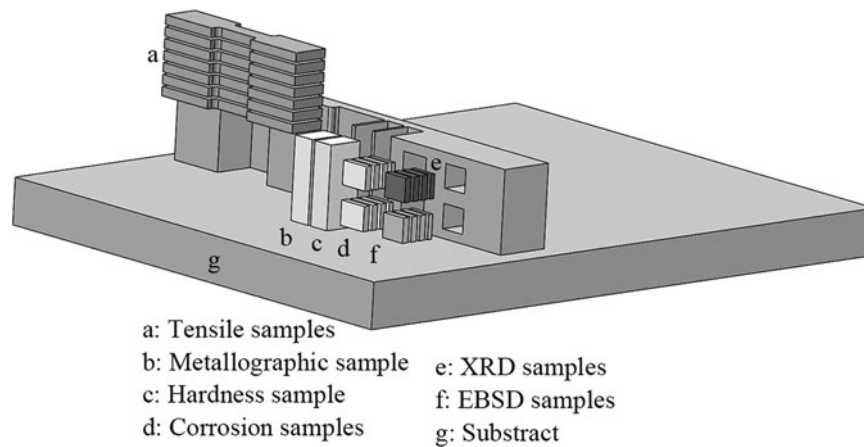


FIG. 2. Schematic showing the location in the Ti-Cu alloys from which the test samples were extracted.

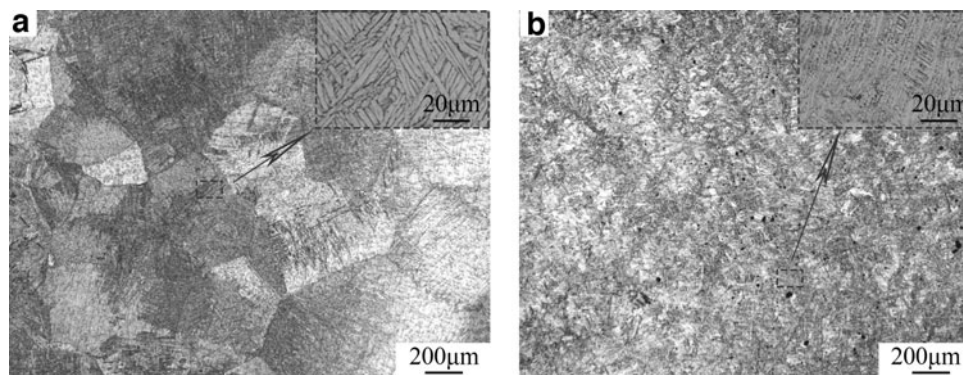


FIG. 3. Optical micrographs of the Ti6-Al4-V substrate (a) and Ti-7.3%Cu alloys (b).

AM) and a wire feeder (WPC-600 feeder machine). The purity of Cu powder (100 mesh size) was >99.9%, which was fed by a powder feeder machine. The purity of Ti wire ( $\geq 99.9\%$ ) with a diameter of 1.2 mm, which was fed by a WPC-600 feeder machine. Ti-Cu alloys composition control is achieved by adjusting the Cu powder feeding amount and Ti wire feeding speed. After many experiments, we selected the best process parameters, as given in Table 1.

The substrate was a  $150 \times 100 \times 10$  mm rolled Ti6-Al4V plate. The as-fabricated sample is shown in Figure 1c. The samples were deposited in a total of four layers with a total height of 15 mm. Owing to the heating instability caused by arc retracting, the fuse is not timely, which makes the two ends of the sample forming quality is not good.

The locations of the printed Ti-Cu alloys from which samples were taken for analysis are shown in Figure 2. The microhardness was measured by an HV-1000 microhardness tester. The phase composition in Ti-Cu alloys was analyzed using X-ray diffraction (XRD). The metallographic sample was etched with hydrofluoric acid solution, and the microstructure was observed by a scanning electron microscope. The grain behavior was studied by electron backscattered diffraction (EBSD). One electrochemical impedance spectroscopy (EIS) electrochemical workstation was used to study the corrosion behavior at room temperature. The 3.5% NaCl corrosion solution was used. The corroded surface was analyzed using a 3D laser microscope OLS4100.

## Results and Discussion

### Microstructure

The microstructures of the Ti-7.3%Cu alloys and Ti-6Al-4V substrate are shown in Figure 3. Figure 3a shows that there is slightly elongated  $\alpha$  grains (light) and intergranular  $\beta$  grains (gray) in the Ti6-Al4-V substrate. The Ti6-Al4-V substrate is cast and rolled. It can be seen from Figure 3a that the structure of the substrate is fine and evenly distributed.

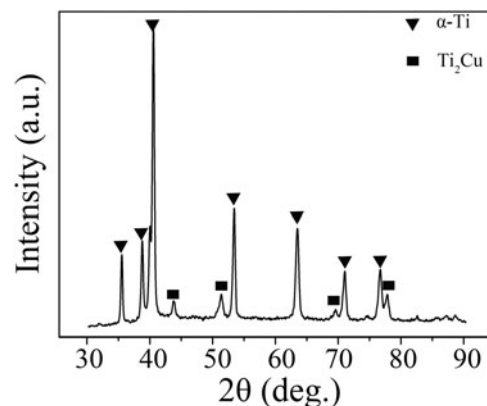


FIG. 4. X-ray diffraction patterns of Ti-7.3%Cu alloys.

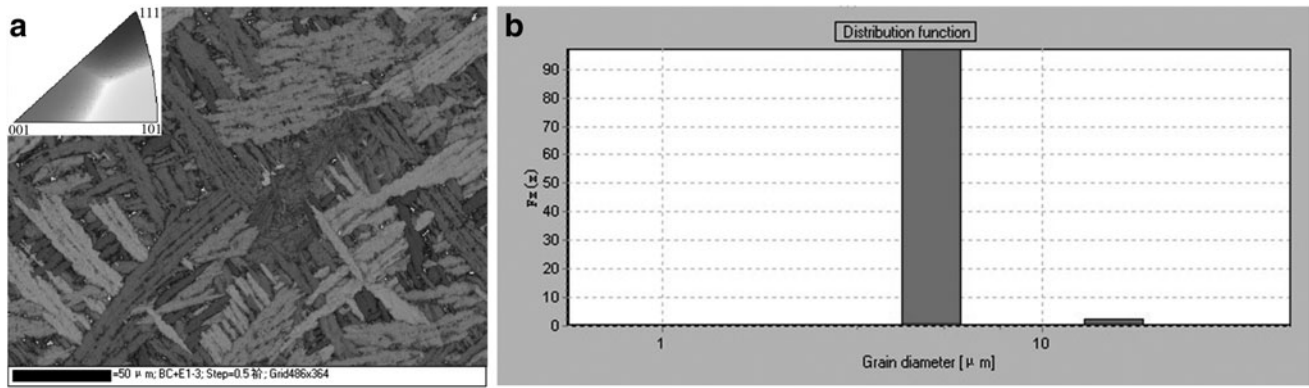


FIG. 5. EBSD inverse pole figures (a), and the grain size distribution (b). EBSD, electron backscattered diffraction.

Figure 3b shows the fine and equiaxed  $\alpha + \text{Ti}_2\text{Cu}$  grains. When the temperature is  $792^\circ\text{C}$ ,  $\beta\text{-Ti}$  will transform into  $\alpha\text{-Ti}$  and  $\text{Ti}_2\text{Cu}$  phases. It is consistent with the XRD test results (Fig. 4).

In general, large columnar crystals will inevitably appear in AM.<sup>32</sup> However, the Ti–7.3%Cu alloys produced by wire + powder synchronous manufacturing have not only large columnar crystals but also fine grains and some equiaxed crystals. To further analyze the microstructure, the EBSD test was performed on the sample, and the results are shown in the Figure 5. The microstructure presents a basket network, and there is also a lamellar structure in the microstructure, and it can be clearly seen that there are fine equiaxed structures (Fig. 5a). According to the statistics of grain size, most grain sizes are  $<10 \mu\text{m}$  (Fig. 5b).

Stjohn et al.<sup>31</sup> found the constitutional supercooling zone is the main factor affecting the grain size according to interdependence theory. The formation of microstructure can be analyzed in combination with Equation (1):

$$\frac{G}{R} \geq \frac{m_l C_0 (K - 1)}{k D_l}, \quad (1)$$

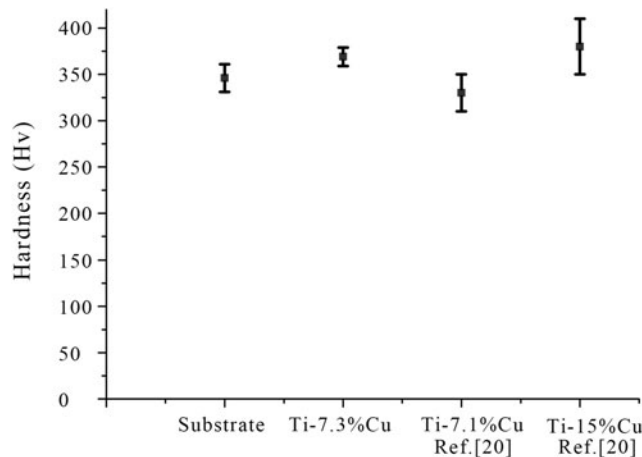


FIG. 6. Hardness of the substrate, Ti–7.3%Cu, Ti–7.1%Cu and Ti–15%Cu.<sup>20</sup>

where  $G$  is temperature gradient,  $R$  the condensation rate,  $m_l$  the absolute value of liquidus slope,  $C_0$  the solute concentration,  $K$  the distribution coefficient, and  $D_l$  the solute diffusion coefficient. When  $G/R$  decreases with the increase of component undercooling, the solidification structure changes from planar crystal to cellular (columnar) crystal. As the two characteristics (high  $G$  and high  $R$ ) of metal AM process and high  $Q$  copper, which promote nucleation ratio. As the component undercooling continues to increase, when it reaches a certain level, a relatively wide undercooling zone will appear in the liquid phase, and at this time, the solidified structure will form equiaxed crystals.

#### Hardness

The bottom is the starting point, and the top is the end point to test the hardness of the alloy. The following hardness results are plotted based on the average results and the error values (Fig. 6). The hardness is measured every 1.5 mm. Six points were detected at the substrate, and eight points were detected at the deposition layer. The average hardness

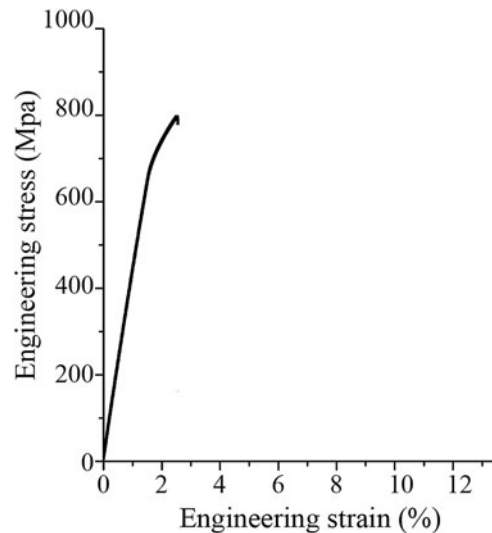


FIG. 7. Representative engineering stress–strain curves of the Ti–7.3%Cu alloys.

TABLE 2. MECHANICAL PROPERTIES OF Ti-Cu ALLOYS

| Alloys (wt.%)                  | YS (MPa) | UTS (MPa) | $\epsilon$ (%) |
|--------------------------------|----------|-----------|----------------|
| Ti-7.3Cu                       | 655 ± 20 | 800 ± 10  | 2.1 ± 0.2      |
| Ti-7.1Cu (Ref. <sup>20</sup> ) | 522 ± 46 | 660 ± 52  | 3.5 ± 0.8      |

$\epsilon$ , uniform elongation; UTS, ultimate tensile strength; YS, yield strength.

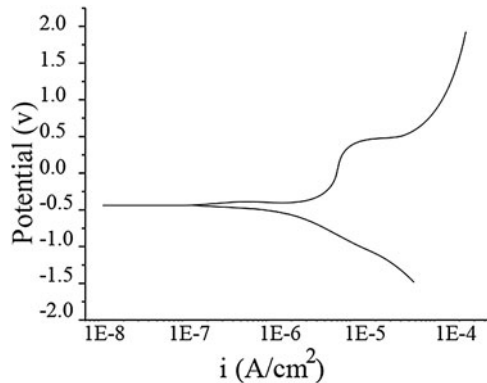


FIG. 8. Potential dynamic curve.

TABLE 3. ELECTROCHEMICAL DATA OF THE Ti-7.3%Cu SAMPLE OBTAINED FROM THE POLARIZATION CURVE

| Sample    | $E_{corr}$ (mV) | $E_{pit}$ (mV) | $I_{corr}$ ( $\mu\text{A}/\text{cm}^2$ ) |
|-----------|-----------------|----------------|--|
| Ti-7.3%Cu | -415            | 275            | 0.21                                     |

$E_{corr}$ , corrosion potential;  $E_{pit}$ , breakdown potential;  $I_{corr}$ , corrosion current density.

obtained for the substrate was  $346 \pm 15$  Hv. For the Ti-7.3%Cu alloy, the average hardness value increased by 6.6% ( $369 \pm 10$  Hv). The hardness values are between those of the cast Ti-7.1%Cu ( $330 \pm 20$  Hv) alloys and the Ti-15%Cu ( $380 \pm 30$  Hv) alloys.<sup>20</sup>

### Tensile properties

The corresponding tensile results are shown in Figure 7. The 0.2% offset yield strength, ultimate tensile strength, and uniform elongation ( $\epsilon$ ) are given in Table 2. It can be seen from the results that the sample has high strength, but low ductility. Its performance is better than that of Ti-7.1Cu alloy cast and heat treated at 900°C for 2 h. Comparing the Ti-7.1Cu, it has higher strength, that is mainly due to the higher volume fraction of eutectoid lamellae  $\alpha$ -Ti, as shown in Figure 4. It has the same ductility as cast Ti-7.1Cu alloys. This is mainly due to the very fine structure of the alloys produced by this method and the achievable transformation of columnar crystals into equiaxed crystals.

### Corrosion resistance

The mentioned analysis shows that the Ti-7.3%Cu alloys made by wire + powder synchronous arc AM had good mechanical properties. Now, the corrosion property of the Ti-7.3%Cu alloys is studied. Figure 8 shows the potentiodynamic polarization curve. The Ti-Cu alloy has an obvious passivation phenomenon in NaCl solution, and the passivation zone is wide, so it has good corrosion resistance. The electrochemical parameters, including corrosion potential ( $E_{corr}$ ), breakdown potential ( $E_{pit}$ ), and corrosion current density ( $I_{corr}$ ), are given in Table 3.

With respect to  $E_{corr}$ , the Ti-7.3%Cu sample showed a more positive  $E_{corr}$  (430 mV) than commercial pure-Ti.<sup>33</sup> Cu can make the passivation film more compact and make the alloy more corrosion resistant. The alloy prepared by wire + powder synchronous arc AM not only has good mechanical properties but also good corrosion resistance.

EIS measurements are performed, and the results are shown in Figure 9. Figure 9a shows the Nyquist diagrams, and Figure 9b and c shows the Bode diagrams. Figure 9b and c shows that the absolute impedance curve in the high-frequency regime ( $10^4$ – $10^5$  Hz) is nearly always related to the phase angle close to 0. This is a typical solution resistance ( $R_s$ ) characteristic. From  $10^3$  to  $10^{-1}$  Hz (medium and low frequency), there are two time constants, as shown in Figure 9b. This may be a two-layer structure of passive film.

As titanium is relatively active, it is easy to form oxides, and according to the report by Roh and Macdonald,<sup>34</sup> when

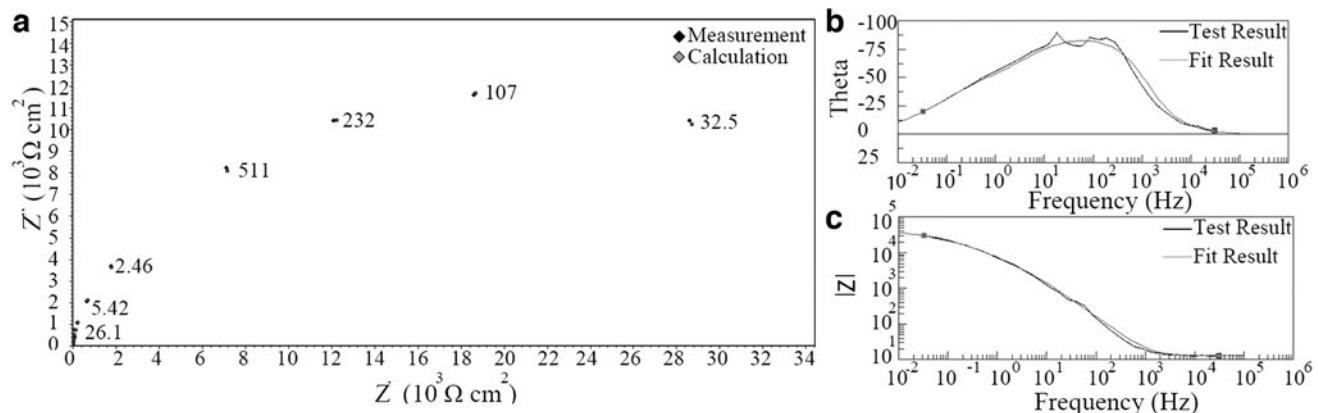


FIG. 9. Nyquist plot diagram (a), Bode phase (b), and Bode plot diagram (c).

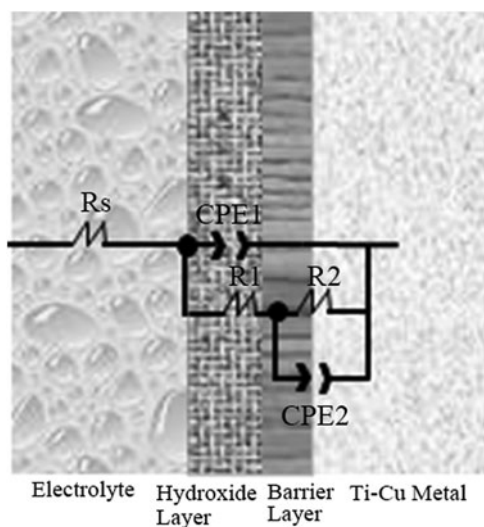


FIG. 10. Equivalent circuit used for fitting the EIS data. EIS, electrochemical impedance spectroscopy.

TABLE 4. EQUIVALENT CIRCUIT PARAMETERS FOR THE ELECTROCHEMICAL IMPEDANCE SPECTROSCOPY SPECTRA OF THE Ti-7.3%Cu SAMPLE

| Parameters                                   | Ti-7.3%Cu              |
|--|------------------------|
| $R_s$ ( $\Omega \cdot \text{cm}^2$ )         | 12.82                  |
| $CPE_1$ ( $\text{F}/\text{cm}^2$ )           | $1.117 \times 10^{-5}$ |
| $R_1$ ( $\text{k}\Omega \cdot \text{cm}^2$ ) | 4.618                  |
| $n_1$ , hydroxide layer                      | 0.98                   |
| $CPE_2$ ( $\text{F}/\text{cm}^2$ )           | $3.818 \times 10^{-5}$ |
| $R_2$ ( $\text{k}\Omega \cdot \text{cm}^2$ ) | 37.17                  |
| $n_2$ , hydroxide layer                      | 0.61                   |
| Chi-squared, $\chi^2$                        | $6.68 \times 10^{-3}$  |

titanium alloy is corroded, two layers of passive film with barrier (inner) layer and outer hydroxide layer will be formed. Based on the mentioned characteristics, an equivalent circuit with two time constants (Fig. 10) was used with ZView<sup>®</sup> software to fit the data.  $R_s$  indicates the resistance of the solution in equivalent circuit. The charge transfer resistance of the hydroxide layer is  $R_1$  and the charge transfer resistance of the barrier layer is  $R_2$ . The impedance of the hydroxide layer is  $CPE_1$ .

The barrier layer is a component of the double layer passive film and its impedance is  $CPE_2$ . By comparing the actual results with the fitting results, the error is within 10%, which shows that the results are reliable. The simulated electrical circuit parameters are summarized in Table 4. From Table 4, the resistance and capacitance of the barrier layer are greater than the resistance and capacitance of the hydroxide layer. This is mainly because the barrier layer formed on the metal surface is relatively stable, whereas the oxide film is unstable, and the oxide film is easily damaged by the electrochemical reaction. The  $R_2$  value reaches  $37,170 \Omega \cdot \text{cm}^2$ , and the  $CPE_2$  value is very small, indicating that the passive film formed is relatively dense and has good corrosion resistance.

To see the surface morphology after corrosion more intuitively, we used a 3D topography instrument to observe the corrosion surface. Figure 11a shows that the surface has been corroded, and the corrosion severity of the entire sample surface is similar, which also indicates that the sample composition is relatively uniform. The number and size of pits are relatively small (Fig. 11b). The seriously corroded parts often form pits, and the expansion of corrosion is the main reason for the change in pit size. The root mean square roughness ( $R_q$ ) of the surface is  $1.106 \mu\text{m}$ . The small height fluctuations shown in Figure 11c also confirm this. The fluctuation amplitude of the selected area is  $2.85 \mu\text{m}$ .

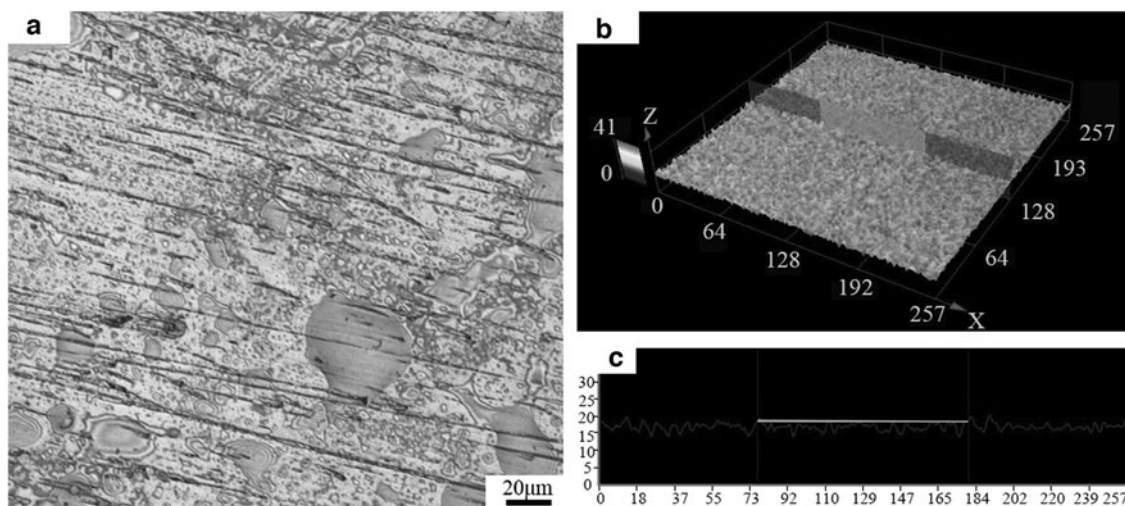


FIG. 11. Surface morphology of the corrosion sample (a), corresponding 3D topography (b), and amplitude curve of the selected section surface height (c).

## Conclusions

In this study, a new wire + powder synchronous arc AM method is proposed to make a Ti-Cu alloy. A sample with a smooth surface and good forming quality was successfully deposited. The microstructure, hardness, tensile properties, and corrosion resistance of the Ti-7.3%Cu alloys were investigated. The conclusions of this article are as follows:

- (1) This method shows great manufacturing potential. The Ti-Cu alloys prepared in this study have no cracks and pores and its properties are better than those of casting alloys.
- (2) Most of the Ti-Cu alloys prepared by this method have a grain size of 10  $\mu\text{m}$ , and have equiaxed crystal formation, which overcomes the generation of large columnar crystal in AM and provides a method to solve the inherent large columnar crystal in AM.
- (3) In the research, an equivalent circuit with two time constants is used. The barrier layer formed on the metal surface is relatively stable, whereas the oxide film is unstable, and the oxide film is easily damaged by electrochemical reactions. The copper can make the passivation film more compact and make the alloy more corrosion resistant.

## Authors' Contributions

All authors have seen and approved the final version of the article. The article is the author's original work and has not been previously published and is not under consideration for publication elsewhere. C.S. and Y.W. contributed equally to this study. C.S. and Y.W. contributed to conceptualization, investigation, methodology, and writing—original draft. W.W. and L.H. tested samples. S.K. was involved in supervision and writing—review and editing. X.C. was involved in supervision and funding acquisition. S.Q. carried out tests and analysis of EBSD, review, and editing.

## Author Disclosure Statement

No conflict of interest exists in the submission of this article, and the article is approved by all authors for publication.

## Funding Information

This study was sponsored by the National Natural Science Foundation of China under Grant number 51975419 and Key Research and Development Program of Zhejiang Province Grant number 2022C01058.

## References

1. Li N, Huang S, Zhang G, et al. Progress in additive manufacturing on new materials: A review. *J Mater Sci Technol* 2019;35(2):242–269; doi: 10.1016/j.jmst.2018.09.002
2. Bandyopadhyay A, Heer B. Additive manufacturing of multi-material structures. *Mater Sci Eng R Rep* 2018;129:1–16; doi: 10.1016/j.mser.2018.04.001
3. Wang Y, Konovalov S, Chen X, et al. Research on plasma arc additive manufacturing of Inconel 625 Ni-Cu functionally graded materials. *Mater Sci Eng A* 2022; 853:143796; doi: 10.1016/j.msea.2022.143796
4. Rodrigues TA, Cipriano Farias FW, Zhang K, et al. Wire and arc additive manufacturing of 316L stainless steel/ Inconel 625 functionally graded material: Development and characterization. *J Mater Res Technol* 2022;21:237–251; doi: 10.1016/j.jmrt.2022.08.169
5. Wu B, Pan Z, Ding D, et al. A review of the wire arc additive manufacturing of metals: properties, defects and quality improvement. *J Manuf Process* 2018;35:127–139; doi: 10.1016/j.jmapro.2018.08.001
6. Cunningham CR, Flynn JM, Shokrani A, et al. Invited review article: Strategies and processes for high quality wire arc additive manufacturing. *Addit Manuf* 2018;22:672–686; doi: 10.1016/j.addma.2018.06.020
7. Williams SW, Martina F, Addison AC, et al. Wire + Arc additive manufacturing. *Mater Sci Technol* 2016;32(7):641–647; doi: 10.1179/1743284715Y.0000000073
8. Bevans B, Ramalho A, Smoqi Z, et al. Monitoring and flaw detection during wire-based directed energy deposition using in-situ acoustic sensing and wavelet graph signal analysis. *Mater Des* 2023;225:111480; doi: 10.1016/j.matdes.2022.111480
9. Zuo X, Zhang W, Chen Y, et al. Wire-based directed energy deposition of NiTiTa shape memory alloys: Microstructure, phase transformation, electrochemistry, X-ray visibility and mechanical properties. *Addit Manuf* 2022;59:103115; doi: 10.1016/j.addma.2022.103115
10. Li S, Li JY, Jiang ZW, et al. Controlling the columnar-to-equiaxed transition during Directed Energy Deposition of Inconel 625. *Addit Manuf* 2022;57:102958; doi: 10.1016/j.addma.2022.102958
11. Wang Y, Chen X, Konovalov S, et al. In-situ wire-feed additive manufacturing of Cu-Al alloy by addition of silicon. *Appl Surf Sci* 2019;487:1366–1375; doi: 10.1016/j.apsusc.2019.05.068
12. Wang Y, Konovalov S, Chen X, et al. Influence of silicon and magnesium on the mechanical properties of additive manufactured Cu-Al alloy. *3D Print Addit Manuf* 2021;8(5):331–339; doi: 10.1089/3dp.2020.0321
13. Martukanitz R, Michaleris P, Palmer T, et al. Toward an integrated computational system for describing the additive manufacturing process for metallic materials. *Addit Manuf* 2014;1:52–63; doi: 10.1016/j.addma.2014.09.002
14. Zheng H, Chen R, Qin G, et al. Microstructure evolution, Cu segregation and tensile properties of CoCrFeNiCu high entropy alloy during directional solidification. *J Mater Sci Technol* 2020;38:1–22; doi: 10.1016/j.jmst.2019.08.019
15. Zhang D, Qiu D, Gibson MA, et al. Additive manufacturing of ultrafine-grained high-strength titanium alloys. *Nature* 2019;576(7785):91–95; doi: 10.1038/s41586-019-1783-1
16. Farayibi PK, Folkes JA, Clare AT. Laser deposition of Ti-6Al-4V wire with WC powder for functionally graded components. *Mater Manuf Process* 2013;28(5):514–518; doi: 10.1080/10426914.2012.718477
17. Li F, Gao Z, Li L, et al. Microstructural study of MMC layers produced by combining wire and coaxial WC powder feeding in laser direct metal deposition. *Opt Laser Technol* 2016;77:134–143; doi: 10.1016/j.optlastec.2015.09.018
18. Sun J, Yu H, Zeng D, et al. Wire-powder-arc additive manufacturing: A viable strategy to fabricate carbide ceramic/aluminum alloy multi-material structures. *Addit Manuf* 2022;51:102637; doi: 10.1016/j.addma.2022.102637
19. Herzog D, Seyda V, Wycisk E, et al. Additive manufacturing of metals. *Acta Mater* 2016;117:371–392; doi: 10.1016/j.actamat.2016.07.019

20. Hayama AOF, Andrade PN, Cremasco A, et al. Effects of composition and heat treatment on the mechanical behavior of Ti-Cu alloys. *Mater Des* 2014;55:1006–1013; doi: 10.1016/j.matdes.2013.10.050
21. Zhang E, Wang X, Chen M, et al. Effect of the existing form of Cu element on the mechanical properties, bio-corrosion and antibacterial properties of Ti-Cu alloys for biomedical application. *Mater Sci Eng C* 2016;69:1210–1221; doi: 10.1016/j.msec.2016.08.033
22. Moniri Javadhesari S, Alipour S, Akbarpour MR. Microstructural characterization and enhanced hardness, wear and antibacterial properties of a powder metallurgy SiC/Ti-Cu nanocomposite as a potential material for biomedical applications. *Ceram Int* 2019;45(8):10603–10611; doi: 10.1016/j.ceramint.2019.02.127
23. Akbarpour MR, Moniri Javadhesari S. Wear performance of novel nanostructured Ti-Cu intermetallic alloy as a potential material for biomedical applications. *J Alloys Compd* 2017;699:882–886; doi: 10.1016/j.jallcom.2017.01.020
24. Yu F, Wang H, Yuan G, et al. Effect of Cu content on wear resistance and mechanical behavior of Ti-Cu binary alloys. *Appl Phys A Mater Sci Process* 2017;123(4):278; doi: 10.1007/s00339-017-0921-6
25. Campo KN, Lopes ESN, Parrish CJ, et al. Rapid quenching of semisolid Ti-Cu alloys: Insights into globular microstructure formation and coarsening. *Acta Mater* 2017;139:86–95; doi: 10.1016/j.actamat.2017.08.006
26. Moniri Javadhesari S, Alipour S, Akbarpour MR. Biocompatibility, osseointegration, antibacterial and mechanical properties of nanocrystalline Ti-Cu alloy as a new orthopedic material. *Colloids Surf B Biointerfaces* 2020;189:110889; doi: 10.1016/j.colsurfb.2020.110889
27. Liu J, Li F, Liu C, et al. Effect of Cu content on the antibacterial activity of titanium-copper sintered alloys. *Mater Sci Eng C* 2014;35(1):392–400; doi: 10.1016/j.msec.2013.11.028
28. Holden FC, Watts AA, Ogden HR, et al. Heat treatment and mechanical properties of Ti-Cu alloys. *JOM* 1955;7(1):117–125; doi: 10.1007/bf03377465
29. Williams JC, Taggart R, Polonis DH. An electron microscopy study of modes of intermetallic precipitation in Ti-Cu alloys. *Metallur Transact* 1971;2(4):1139–1148; doi: 10.1007/BF02664246
30. Zhang D, Sun S, Qiu D, et al. Metal alloys for fusion-based additive manufacturing. *Adv Eng Mater* 2018;20(5):1700952; doi: 10.1002/adem.201700952
31. Stjohn DH, Qian M, Easton MA, et al. The Interdependence Theory: The relationship between grain formation and nucleant selection. *Acta Mater* 2011;59(12):4907–4921; doi: 10.1016/j.actamat.2011.04.035
32. Dong B, Pan Z, Shen C, et al. Fabrication of copper-rich Cu-Al alloy using the wire-arc additive manufacturing process. *Metallur Mater Transact B* 2017;48(6):3143–3151; doi: 10.1007/s11663-017-1071-0
33. Wang J, Zhang S, Sun Z, et al. Optimization of mechanical property, antibacterial property and corrosion resistance of Ti-Cu alloy for dental implant. *J Mater Sci Technol* 2019;35(10):2336–2344; doi: 10.1016/j.jmst.2019.03.044
34. Roh B, Macdonald DD. Passivity of titanium: Part II, the defect structure of the anodic oxide film. *J Solid State Electrochem* 2019;23(7):1697–1979; doi: 10.1007/s10008-019-04254-0

Address correspondence to:

*Xizhang Chen*  
*Zhejiang Provincial Key Laboratory*  
*of Laser Processing Robotics*  
*College of Mechanical and Electrical Engineering*  
*Wenzhou University*  
*Wenzhou 325035*  
*Zhejiang*  
*China*

*E-mail:* kernel.chen@gmail.com

*Shuyang Qin*  
*National Engineering Research Center for Equipment*  
*and Technology of Cold Strip Rolling*  
*Yanshan University*  
*Qinhuangdao 066004*  
*Hebei*  
*China*

*E-mail:* qin@ysu.edu.cn